ARTICLE

doi:10.1038/nature24054

Pumping liquid metal at high temperatures up to 1,673 kelvin

C. Amy[1], D. Budenstein[1], M. Bagepalli[1], D. England[1], F. DeAngelis[1], G. Wilk[1], C. Jarrett[1], C. Kelsall[1], J. Hirschey[1], H. Wen[1], A. Chavan[1], B. Gilleland[1], C. Yuan[1], W. C. Chueh[2], K. H. Sandhage[3,4], Y. Kawajiri[5] & A. Henry[1,3,6]

Heat is fundamental to power generation and many industrial processes, and is most useful at high temperatures because it can be converted more efficiently to other types of energy. However, efficient transportation, storage and conversion of heat at extreme temperatures (more than about 1,300 kelvin) is impractical for many applications. Liquid metals can be very effective media for transferring heat at high temperatures, but liquid–metal pumping has been limited by the corrosion of metal infrastructures. Here we demonstrate a ceramic, mechanical pump that can be used to continuously circulate liquid tin at temperatures of around 1,473–1,673 kelvin. Our approach to liquid–metal pumping is enabled by the use of ceramics for the mechanical and sealing components, but owing to the brittle nature of ceramics their use requires careful engineering. Our set-up enables effective heat transfer using a liquid at previously unattainable temperatures, and could be used for thermal storage and transport, electric power production, and chemical or materials processing.

Thermal energy has an indispensable role in modern society. Virtually every energy conversion process creates heat as a product or by-product, making it one of the most abundant forms of energy. Of particular importance is the conversion of heat into more useful forms of energy, such as mechanical or electrical work or the potential energy stored in chemical bonds. Thermal energy is of greatest value—that is, has the highest available work or 'exergy'—when it can be transported, stored and converted at the highest possible temperatures. However, the manipulation of heat at extreme temperatures (well above 1,300 K) has proven to be extremely difficult for many applications. Even in cases where high-temperature fluids are used, such as gas turbines and rocket engines, the pumps and compressors are not operated at high temperatures. Instead, the pumps and compressors are kept in a relatively cold portion of the system, with mechanical force transmitted through the fluid itself to the hot region. Very few applications involve the flow of high-temperature liquids. The high-temperature pumping of liquids is severely restricted by limitations on pump materials because there are only a few classes of materials that remain solid, are chemically stable with such liquids, possess sufficient strength and exhibit long life at temperatures well above 1,300 K.

Molten metals can be optimal high-temperature heat-transfer fluids because they: (1) tend to have low viscosities near their liquidus temperatures; (2) have high electrical conductivity and therefore high thermal conductivity (because convective heat transfer is directly proportional to thermal conductivity, the use of molten metals instead of fluids such as oils and salts that are electrically insulating can result in an increase in the heat transfer coefficient of two to three orders of magnitude); (3) can have a very large liquid range (for example, 505–2,876 K for tin), thereby enabling single-phase operation and high volumetric energy density via sensible heating; and (4) can be relatively abundant (mass-produced) and inexpensive[1,2]. These desirable properties lead to compact and high-volumetric-power-density heat transfer and thermal storage. Other heat-transfer media and approaches (such as molten salts or glasses, fluidized solids, gases and radiation) have disadvantages including temperature limitations below 1,300 K (for example, molten salts[2–4]), high pumping power requirements due to high viscosity and low thermal conductivity (for example, molten glasses[2,5,6]), geometric constraints (for example, radiation[7]), and low densities or convective heat-transfer coefficients (for example, gases and fluidized solids).

Liquid–metal containment

Although highly attractive, liquid-metal heat transfer has historically been limited by the availability of suitable containment materials. For example, liquid tin reacts with and/or acts as a solvent for nearly all metals. At high temperatures, mass diffusion and reaction kinetics are accelerated, so piping or containment infrastructures made of conventional structural metals degrade rapidly in contact with hot liquid tin[8–11]. Another class of materials that could be used is ceramics, although these materials (defined broadly here as inorganic, non-metallic materials) are usually disregarded owing to their brittle nature[12,13]. The expectation has been that if ceramics are used (for example, in a mechanical pump) they will crack and fail, owing to their low fracture toughness, whenever they experience non-compressive loads. Although they potentially require high energy for manufacturing, their brittle nature is their main drawback and it is therefore worthwhile considering ways of overcoming this issue to potentially realize important advances.

Certain ceramics can retain their mechanical stiffness at extreme temperatures (>1,300 K)[14–16] and be thermodynamically stable with respect to hot liquid metals (such as Sn, Pb, Bi, Al and Si)[17,18]. The notion of thermodynamic stability used here is important to emphasize, because it corresponds to a fundamentally different condition for operation from that used in many applications. Often, there is a thermodynamic driving force for reaction, but a kinetically limiting step prevents the reaction from occurring at a substantial rate[18]. In some cases, such as concentrated solar power, a driving force for reaction exists (between the molten salt and stainless steel infrastructure) that restricts the temperature and lifetime because kinetics accelerate to an unacceptable rate above 840 K (ref. 19). By using thermodynamically compatible materials, we need not be concerned that a chemical

[1]George W. Woodruff School of Mechanical Engineering, Georgia Institute of Technology, Atlanta, Georgia 30332, USA. [2]Department of Materials Science and Engineering, Stanford University, Stanford, California 94305, USA. [3]School of Materials Science and Engineering, Georgia Institute of Technology, Atlanta, Georgia 30332, USA. [4]School of Materials Engineering, Purdue University, West Lafayette, Indiana 47907, USA. [5]School of Chemical and Biomolecular Engineering, Georgia Institute of Technology, Atlanta, Georgia 30332, USA. [6]Heat Lab, Georgia Institute of Technology, Atlanta, Georgia 30332, USA.

degradation mechanism could become exacerbated with time (for example, owing to the loss of a protective layer or barrier). Instead, the key question is whether clever approaches that use ceramics—which accommodate their brittle nature—can be developed to pump and circulate liquid metals at extreme temperatures. This is an important question to address because a technology that enables liquid-metal pumping and heat transfer above 1,300 K would unlock new strategies and concepts in, for example, electric power generation and chemical and metals processing (see section 'Discussion and conclusion')[7,17,20–27].

The remainder of this Article describes the key features and successful testing of an entirely ceramic pump operating at a steady-state temperature of 1,473 K, with peak temperatures above 1,673 K. The design of the pump system and experimental set-up is included in Methods. The pump is the key component to demonstrate because it enables transport of the fluid and is subject to the most challenging thermal, mechanical and chemical conditions and constraints in the entire circulation loop; that is, it is subject to dynamic and tensile loading, a corrosive and abrasive environment, and large thermal gradients. The most notable challenge with mechanical pumping is dynamic sealing. Although it is possible to pump liquid metals electromagnetically, with no moving parts (and therefore no dynamic seals), such approaches face substantial unresolved challenges[28,29]. Given these considerations, our approach focused on: (1) overcoming the issue of using brittle ceramics in rotating machinery and (2) demonstrating the ability to seal liquid tin above 1,300 K. The key innovations developed in this work are the prototype pump design (developed with the aid of modern modelling and fabrication techniques) and the selection of appropriate materials for greatly reduced likelihood of failure under the operational conditions used. Although the refractory nature of ceramics has been well known for centuries, the more modern ability to precisely fabricate and machine advanced ceramics and composites and to simulate their mechanical, thermal and chemical behaviour is what has enabled this advancement.

Prototype system

On the basis of the practical limits of heaters and insulation, and the stability of certain ceramics of interest, we targeted a nominal temperature of about 1,473 K for this prototype. However, the main design principles and phenomena are not limited to this temperature, and it is possible to create a system that operates at even higher temperatures. To achieve this high-temperature operation, an inert N_2 atmosphere was used, which can also be used at the industrial scale[30–32] (see Methods, Extended Data Figs 1 and 2). This inert environment enabled the use of materials such as graphite and tungsten, which do not form stable compounds with tin[33,34]. Nonetheless, the design did not leverage the fact that tungsten is compatible with tin, because tungsten was not exposed to the liquid metal and, in general, no metals need to be exposed to the liquid metal in our approach. Graphite was used for piping, joints and seals, and tungsten was used outside of the sealed region, where tensile forces were applied. We selected Shapal Hi-M Soft as the primary pump material. Shapal is a machinable aluminium-nitride-rich composite (80% AlN, 20% BN) with a similar coefficient of thermal expansion to the graphite that we used (about $5 \times 10^{-6}\,K^{-1}$). Hence, reliable, thermal-expansion-matched joints could be achieved between graphite and Shapal.

An external gear pump was selected for the pump type because of several fundamental attributes, namely, its ability to deliver very high pressure over a wide range of flow rates and because the supplied pressure depends minimally on the fluid momentum and viscosity, which is important for many applications[35,36]. External gear pumps use the meshing of gears to pump fluid that is trapped between the teeth around the outside of the gears, as shown on the right of Fig. 1; an overview of the system is shown on the left of Fig. 1. Because the two gears remain in contact, fluid cannot return through the centre, so it is forced to the outlet. A straight, involute, spur-tooth geometry was used for ease of machining.

The extreme-temperature pump experiences substantial misalignment due to thermal expansion, with more than 1 mm of vertical growth (Fig. 2d). To minimize misalignment, the pump and motor were intentionally misaligned in the vertical direction at room temperature to account for expansion when the pump was at high temperature. This approach was complemented by the angularly flexible, yet radially constrained, shaft set-up, which involves a tungsten sleeve bearing (see Methods).

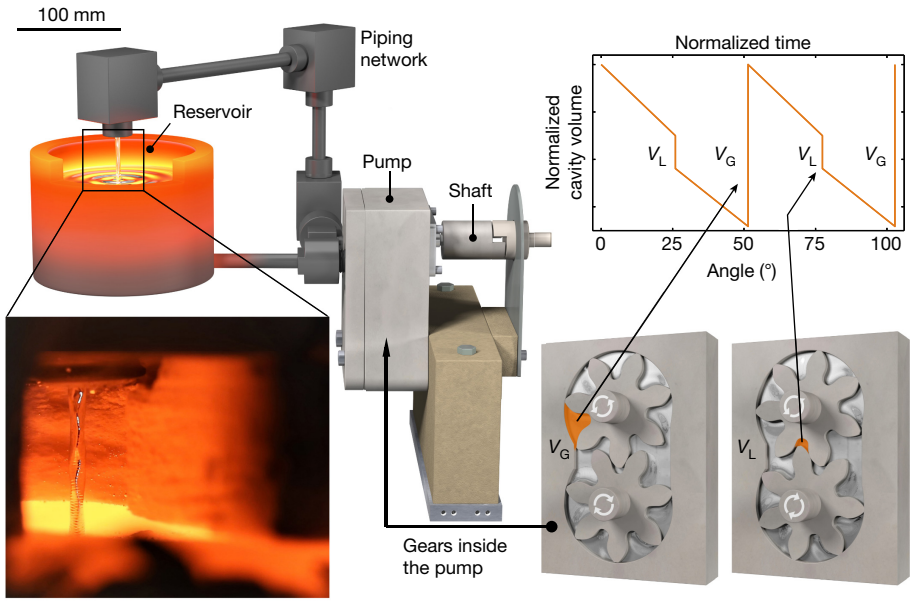

Figure 1 | Model of the pump. A graphite reservoir primes the pump (left). The gears then pressurize the fluid, causing it to flow through the graphite piping where it then falls back into the reservoir. An image showing tin flowing at 1,673 K is provided bottom left. A model of the pump gears is shown on the right, illustrating the direction of rotation, with a plot showing how the volume near the outlet changes with rotation. The two discontinuities are transitions at which the volume highlighted in orange is gained (V_G) and then lost (V_L). The slope of the volume versus angle or time is the theoretical volumetric flow rate for an incompressible fluid.

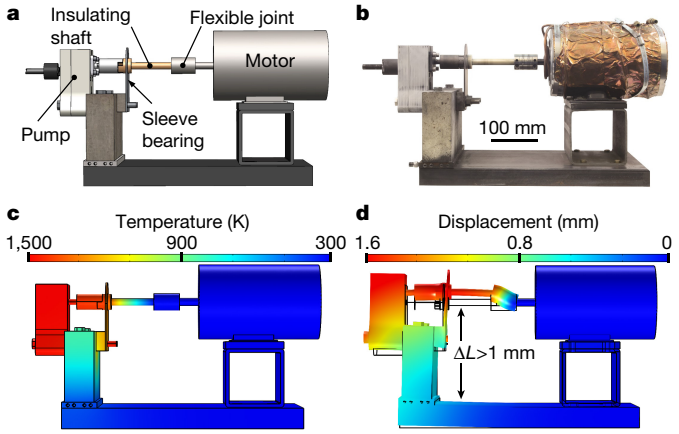

Figure 2 | Pump design, analysis and fabrication. a, Model of the pump system, identifying key components. **b**, Photograph of the pump system. **c**, Thermal model of the pump system, showing the predicted temperature distribution for the set-up when heated. **d**, Thermal strain model of the pump system (enhanced by a factor of 15), used to illustrate the displacement due to thermal expansion and to assess the stresses that develop in different components.

As mentioned above, the most notable issue with attempting to make a mechanical pump for extreme temperatures is sealing. Pump seals are typically made from polymers, owing to their high compliance against sealing surfaces, but polymers are restricted to much lower temperatures than the target here (1,473 K). Instead, we exploited the property of graphite that made it unfavourable as a pump construction material: its low strength. Graphite is similar to polymers in that it is characterized by mixed chemical bonding. Polymers contain stiff intramolecular interactions that make them resistant to corrosion, but weak van der Waals interactions between molecules allow the polymer chains to easily slide and deform to accommodate sealing surfaces. Similarly, graphite consists of stiff intramolecular bonds in each graphene layer, with much weaker van der Waals bonds between layers, allowing substantial deformation. In Fig. 3 we show two examples of the graphite seals that we developed, which both rely on the axial compression of graphite to create a seal through radial expansion (see Methods). Conceptually, other refractories, such as hexagonal boron nitride, with a similar crystal structure or bond heterogeneity to graphite could also serve as a sealing material, and in some applications sealless sump pumps can be used instead[37,38].

Once a sealed circulation loop was made, as shown in Fig. 1, several initial experiments were conducted, without measuring the flow rate. Instead, the liquid-metal stream that exited the outlet pipe directly was observed through a viewing port cut into the insulation and a window installed on the inert chamber. Subsequent experiments used a flow meter to quantify the flow rate (see Methods). This flow meter was visual in that it indicated a flow-rate range on the basis of the number of visible fluid streams (see Methods).

Results

The pump system, including a reservoir, visual flow meter, necessary piping and joints, was tested for 72 h at an average temperature of 1,473 K (Fig. 4 and Supplementary Video). This temperature limit was a result of limited heater power and is not a fundamental bound on the pump or other system components. The flow meter viewport resulted in substantial loss of radiative heat, which limited the steady-state temperature of the system. Flow from two streams as seen from the viewport is shown in Fig. 4 and a view of the experiment chamber is provided in Extended Data Fig. 2.

A flow rate of 24–108 g s^{-1} was maintained for the first 60 h of the test (see Methods, Extended Data Figs 3 and 4 for the design of the flow meter). Although this flow rate is small, it corresponds to a heat transfer rate of about 5–20 kW for liquid tin heated from 573 K to 1,473 K.

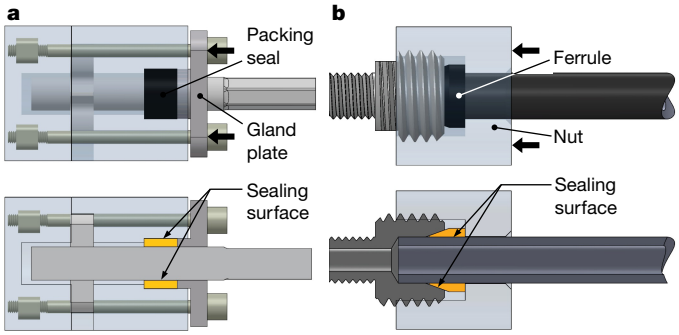

Figure 3 | Sealing methods. Both seals work under the basic principle that when the graphite is compressed axially (indicated by the bold black arrows), because it is soft, it expands radially, pressing compliantly against the sealing surfaces. **a**, Graphite-packing shaft seal for sealing against rotating components. **b**, Graphite-ferrule-based fluid seal between two stationary pipes.

For a pump operated at 1,800 r.p.m., this would increase to about 750 kW. Furthermore, if the gear diameter (3.8 cm) and thickness (1.3 cm) were scaled up by a factor of about 4.5, then the heat transfer rate would be about 100 MW. Therefore, because of the high volumetric energy density of tin, this small-scale pump can be reasonably scaled up to the typical capacity of a full-scale power plant with an increase of less than one order of magnitude in dimensions.

The initial spike in temperature was driven by auxiliary Kanthal pre-heaters, which have a very short life at this temperature. As a result, they failed and the remaining heat was supplied by the induction furnace loop around the reservoir, which spread through the system via the flowing liquid tin. In addition, convective cooling of the ambient gas inside the inert containment system was reduced after 25 h, which enabled a slight increase in temperature (visible in Fig. 4) to the 1,473 K target. After 55 h, a decrease in flow rate occurred and the rotational speed of the pump was temporarily increased to maintain the target flow rate. The pump continued to operate, and the test was stopped after 72 h for post-operation analysis. There was no mechanical failure of any components during the test, nor was there failure upon cooling (at a rate of 1–5 K min^{-1}).

The gear teeth in the pump experienced visible wear (Fig. 5), although the sleeve bearings did not wear noticeably. Whereas the highest volume of wear occurred on the gear teeth, the wear at the radial gear tips is the most detrimental because it allows fluid to leak around the teeth (see Extended Data Fig. 5 and Extended Data Table 1 for geometry and wear rates, respectively). The outer surface of the radial gear tips can contact the pump body only if the shaft or bearings wear; hence, minimizing the wear rates of the shaft and bearing is key. Although a wear-resistant (hard, fine-grain) ceramic should replace Shapal[39], which was selected for machinability rather than wear performance (low hardness of 380 kg mm^{-2} HV, where HV is the

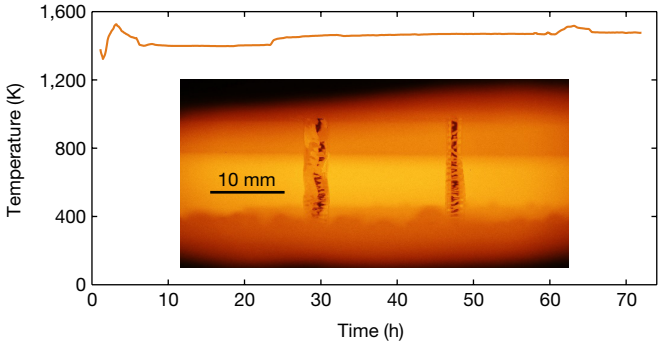

Figure 4 | Pump temperature (main panel) and representative flow from the visual flow meter (inset). The presence of two streams indicates a flow rate of 28–108 g s^{-1}. Data are provided as Supplementary Data 1.

Figure 5 | Wear on Shapal gear teeth after 72 h of continuous pumping. The black outline behind the drive gear indicates the original shape. The yellow shading and arrows highlight the width loss of about 1 mm.

Vickers pyramid number, about 20% of the hardness of aluminium oxide), a large reduction in the wear rate could also be achieved by improving other tribological conditions[40]. For example, as detailed in Methods, shaft wear was reduced by more than an order of magnitude from earlier tests simply by polishing the shafts. Further design improvements to extend the life by several orders of magnitude, with negligible wear, are discussed in Methods and should enable many years of continuous operation.

Before the flow-metered experiment at 1,473 K, we successfully conducted other tests at temperatures as high as 1,673 K, with excursions up to 1,773 K. These higher temperatures were achievable because the flow meter was not present, which reduced the system size and corresponding heat loss. Even so, on the basis of visual comparisons with the metered tests, the flow rate in each of these earlier tests was estimated to be more than 20 g s^{-1}. An image from the test that achieved the highest temperature is included in Fig. 1, in which the width of the flow stream width (about 3 mm) can be seen to be similar to that obtained with the visual- and weight-based flow meters.

Discussion and conclusion

We have designed, fabricated and successfully tested an entirely ceramic pump, demonstrating the highest-temperature pumping of any liquid ever achieved. We pumped liquid tin at temperatures in excess of 1,673 K without failure of any system components; a pathway to realizing the long life for these components that is required in industrial settings is described in Methods. The ability to pump liquid metal at high temperatures is particularly important because liquid metals have low viscosity and high thermal conductivity, enabling the use of compact and efficient components within the pumping system. Collecting, transporting, storing and converting heat above 1,300 K has previously been restricted to more cumbersome or limiting means (for example, relying on either thermal radiation or convection via gases). However, with our approach, many new concepts are now possible.

For example, concentrated solar power at twice the currently achievable peak temperature is enabled[26,41], which could result in a relative increase in efficiency of approximately 50%, reducing costs by 20%–30% (refs 2, 42). Concentrated solar power is particularly attractive, given that lower-temperature (973–1,073 K) approaches to solar power are predicted to achieve cost parity with natural gas[43,44]. Moreover, our approach could enable high-exergy thermal energy storage[23] and new solar fuels concepts[45]. Although non-intuitive, this technology could even make thermal energy grid storage economically viable, which could become very profitable if non-dispatchable renewables increase in market share[46]. There are several on-going efforts to commercialize thermal energy grid storage, in both industry and academia. By operating at the extreme temperatures that are enabled by our technology, the efficiency of such a system can reach 60% (ref. 26), which would make the economics competitive with low-cost resources, such as pumped hydroelectric storage.

Other new and innovative components, such as direct-contact liquid-droplet heat exchangers, are also enabled by our approach. For example, liquid tin could be used to transfer heat to and from a noble gas such as helium[2,21,22]. Such heat exchangers can be extremely efficient and can even enable accession of the heat of solidification[47], which is particularly large for materials such as silicon (1.92 MJ kg^{-1})[26]. Just as liquid metals can help to transport and store energy, they can also enable improvements to existing power cycles. For example, in gas turbines, where up to 5% of efficiency is lost from cooling of the turbine blades[48], liquid metals could be used to cool turbine blades more efficiently and could even enable recuperation of this heat. Similarly, our technology could make thermophotovoltaic solid-state thermal-to-electricity conversion competitive as a concentrated solar power heat engine[26] or for thermal energy grid storage. Furthermore, many industrial processes occur at high temperatures[7,24,25,27,49] and could be made more efficient or effective by making use of the ability to pump liquid metal at extreme temperatures. For example, high-pressure injection moulding of metal alloys can increase the speed and quality of castings, with less oxidation and without the geometric limits of current methods[24]. Similarly, pumping enables precise control over the cooling rate in single-crystal super-alloy castings to optimize the final properties[49]. There are also industries, such as aluminium processing[25,27], in which high-temperature waste heat is available and could be recovered and internally recycled or converted to electricity to ultimately reduce costs.

On the basis of these results and this initial proof-of-concept demonstration, the use of ceramic and refractory metal components in an inert atmosphere should now be considered a viable approach to pumping liquid metal at extreme temperatures. This technology has broad applications and it is important to begin to rethink how various industries operate, to identify opportunities where substantial energy savings or increases in efficiency could be achieved.

Online Content Methods, along with any additional Extended Data display items and Source Data, are available in the online version of the paper; references unique to these sections appear only in the online paper.

Received 23 May; accepted 30 August 2017.

1. Lorenzin, N. & Abánades, A. A review on the application of liquid metals as heat transfer fluid in concentrated solar power technologies. *Int. J. Hydrogen Energy* **41,** 6990–6995 (2016).
2. Wilk, G. *Liquid Metal Based High Temperature Concentrated Solar Power: Cost Considerations.* MSc thesis, Georgia Institute of Technology (2016).
3. Nunes, V. M. B., Queirós, C. S., Lourenço, M. J. V., Santos, F. J. V. & Nieto de Castro, C. A. Molten salts as engineering fluids. *Appl. Energy* **183,** 603–611 (2016).
4. Fritsch, A. *et al.* Conceptual study of central receiver systems with liquid metals as efficient heat transfer fluids. *Energy Procedia* **69,** 644–653 (2015).
5. Elkin, B., Finkelstein, L., Dyer, T. & Raade, J. Molten oxide glass materials for thermal energy storage. *Energy Procedia* **49,** 772–779 (2014).
6. Cárdenas, B., León, N., Pye, J. & García, H. D. Design and modelling of a high temperature solar thermal energy storage unit based on molten soda lime silica glass. *Solar Energy* **126,** 32–43 (2016).
7. Elliott, A. J. & Pollock, T. M. Thermal analysis of the Bridgman and liquid-metal-cooled directional solidification investment casting processes. *Metall. Mater. Trans. A* **38,** 871–882 (2007).
8. Plevan, M. *et al.* Thermal cracking of methane in a liquid metal bubble column reactor: experiments and kinetic analysis. *Int. J. Hydrogen Energy* **40,** 8020–8033 (2015).
9. Fazio, C. & Balbaud, F. in *Structural Materials for Generation IV Nuclear Reactors* (ed. Yvon, P.) 23–74 (Elsevier, 2017).
10. Legkikh, A. Y., Askhadullin, R. S. & Sadovnichiy, R. P. Ensuring the corrosion resistance of steels in heavy liquid metal coolants. *Nuclear Energy Technol.* **2,** 136–141 (2016).
11. Emmerich, T. & Schroer, C. Corrosion in austenitic steels and nickel-based alloys caused by liquid tin at high temperature. *Corros. Sci.* **120,** 171–183 (2017).
12. Danzer, R. On the relationship between ceramic strength and the requirements for mechanical design. *J. Eur. Ceram. Soc.* **34,** 3435–3460 (2014).
13. Henry, A. & Prasher, R. The prospect of high temperature solid state energy conversion to reduce the cost of concentrated solar power. *Energy Environ. Sci.* **7,** 1819–1828 (2014).
14. Opeka, M. M., Talmy, I. G., Wuchina, E. J., Zaykoski, J. A. & Causey, S. J. Mechanical, thermal, and oxidation properties of refractory hafnium and zirconium compounds. *J. Eur. Ceram. Soc.* **19,** 2405–2414 (1999).

15. Opeka, M. M., Talmy, I. G. & Zaykoski, J. A. Oxidation-based materials selection for 2000°C + hypersonic aerosurfaces: theoretical considerations and historical experience. *J. Mater. Sci.* **39,** 5887–5904 (2004).
16. Fahrenholtz, W. G. & Hilmas, G. E. Ultra-high temperature ceramics: materials for extreme environments. *Scr. Mater.* **129,** 94–99 (2017).
17. Frazer, D., Stergar, E., Cionea, C. & Hosemann, P. Liquid metal as a heat transport fluid for thermal solar power applications. *Energy Procedia* **49,** 627–636 (2014).
18. Pacio, J. & Wetzel, T. Assessment of liquid metal technology status and research paths for their use as efficient heat transfer fluids in solar central receiver systems. *Sol. Energy* **93,** 11–22 (2013).
19. Vignarooban, K., Xu, X., Arvay, A., Hsu, K. & Kannan, A. M. Heat transfer fluids for concentrating solar power systems – a review. *Appl. Energy* **146,** 383–396 (2015).
20. Weeks, J. R. Lead, bismuth, tin and their alloys as nuclear coolants. *Nucl. Eng. Des.* **15,** 363–372 (1971).
21. Bruckner, A. P. & Mattick, A. T. High effectiveness liquid droplet/gas heat exchanger for space power applications. *Acta Astronaut.* **11,** 519–526 (1984).
22. Welty, J. R. in *Direct-Contact Heat Transfer* (eds Kreith, F. & Boehm, R. F.) 197–201 (Springer, 1988).
23. Gur, I., Sawyer, K. & Prasher, R. Searching for a better thermal battery. *Science* **335,** 1454–1455 (2012).
24. Kapranos, P., Carney, C., Pola, A. & Jolly, M. in *Comprehensive Materials Processing* Vol. 5 (eds Hashmi, S. *et al.*) 39–67 (Elsevier, 2014).
25. Thekdi, A. C. & Nimbalkar, S. U. *Industrial Waste Heat Recovery: Potential Applications, Available Technologies and Crosscutting R&D Opportunities.* Report No. ORNL/TM-2014/622 (Oak Ridge National Laboratory, 2015).
26. Seyf, H. R. & Henry, A. Thermophotovoltaics: a potential pathway to high efficiency concentrated solar power. *Energy Environ. Sci.* **9,** 2654–2665 (2016).
27. Yang, W. *et al.* Thermodynamics analysis of carbothermal-chlorination reduction in aluminum production. *Appl. Therm. Eng.* **111,** 876–883 (2017).
28. Dong, X., Huang, X., Liu, L., He, L. & Li, P. A liquid aluminum alloy electromagnetic transport process for high pressure die casting. *J. Mater. Process. Technol.* **234,** 217–227 (2016).
29. Kim, H. R. & Lee, Y. B. A design and characteristic experiment of the small annular linear induction electromagnetic pump. *Ann. Nucl. Energy* **38,** 1046–1052 (2011).
30. Bodbodak, S. & Moshfeghifar, M. in *Eco-Friendly Technology for Postharvest Product Quality* (ed. Siddiqui, M. W.) 39–76 (Academic Press, 2016).
31. Thompson, A. K. *Fruit and Vegetable Storage* 21–36 (Elsevier, 2016).
32. Zhao, H. & Woods, R. in *Advances in Brazing* (ed. Sekulic, D. P.) 280–322 (Woodhead Publishing, 2013).
33. Oden, L. L. & Gokcen, N. A. Sn-C and Al-Sn-C phase diagrams and thermodynamic properties of C in the alloys: 1550 °C to 2300 °C. *Metall. Trans. B* **24,** 53–58 (1993).
34. Pietzka, M. A. & Schuster, J. C. Phase equilibria of the quaternary system Ti/Al/Sn/N at 900 °C. *J. Alloys Compd.* **247,** 198–201 (1997).
35. Beebe, R. S. *Predicitive Maintenance of Pumps Using Condition Monitoring* 155–161 (Elsevier, 2004).
36. Forsthoffer, W. E. *Forsthoffer's Best Practice Handbook for Rotating Machinery* 25–91 (Butterworth-Heinemann, 2011).
37. Hill, R. F. Boron nitride seal and method of use. US patent 5,678,832 (1997).
38. Nesbitt, B. (ed.) *Handbook of Pumps and Pumping* 1–54 (Elsevier, 2006).
39. Milak, P. C., Minatto, F. D., De Noni, A. Jr & Montedo, O. R. K. Wear performance of alumina-based ceramics — a review of the influence of microstructure on erosive wear. *Ceramica* **61,** 88–103 (2015).
40. Hutchings, I. & Shipway, P. *Friction and Wear of Engineering Materials* 1–5 (Butterworth-Heinemann, 2017).
41. DeAngelis, A. *Analysis and Design of a High Temperature Liquid Metal Solar Thermal Receiver* MSc thesis, Georgia Institute of Technology (2016).
42. Dowling, A. W., Zheng, T. & Zavala, V. M. Economic assessment of concentrated solar power technologies: a review. *Renew. Sustain. Energy Rev.* **72,** 1019–1032 (2017).
43. *SunShot Vision Study*. Report No. DOE/GO-102012–3037 (US Department of Energy, 2012).
44. *On the Path to SunShot*. Report No. DOE/EE 1412 (US Department of Energy, 2016).
45. Yuan, C., Jarrett, C., Chueh, W., Kawajiri, Y. & Henry, A. A new solar fuels reactor concept based on a liquid metal heat transfer fluid: reactor design and efficiency estimation. *Sol. Energy* **122,** 547–561 (2015).
46. Sioshansi, R., Denholm, P., Jenkin, T. & Weiss, J. Estimating the value of electricity storage in PJM: arbitrage and some welfare effects. *Energy Econ.* **31,** 269–277 (2009).
47. Cascella, F. & Teyssedou, A. Modeling a direct contact heat exchanger used in a supercritical water loop. *Appl. Therm. Eng.* **79,** 132–139 (2015).
48. Wilcock, R. C., Young, J. B. & Horlock, J. H. The effect of turbine blade cooling on the cycle efficiency of gas turbine power cycles. *J. Eng. Gas Turbines Power* **127,** 109–120 (2005).
49. Brundidge, C. L., Miller, J. D. & Pollock, T. M. Development of dendritic structure in the liquid-metal-cooled, directional-solidification process. *Metall. Mater. Trans. A* **42,** 2723–2732 (2011).

Supplementary Information is available in the online version of the paper.

Acknowledgements We acknowledge funding support from the Advanced Research Projects Agency – Energy (ARPA-E) (DE-AR0000339). We also acknowledge the support of Y. Zhang, B. Capps, A. Robinson and M. Faniel.

Author Contributions C.A., D.B. and M.B. performed the experiments, and A.H., D.E., F.D., G.W., C.K., J.H., H.W., B.G. and A.C. provided assistance. C.A. analysed the data and performed the simulations, and M.B. provided review and assistance. A.H. and D.E. supervised the project. K.H.S., C.J., C.Y., D.E., W.C.C. and Y.K. performed modelling and materials testing. C.A. drafted the majority of the manuscript, and A.H. provided chief contributions. K.H.S., D.B. and M.B. also edited extensively. All authors wrote and reviewed the manuscript.

Author Information Reprints and permissions information is available at www.nature.com/reprints. The authors declare no competing financial interests. Readers are welcome to comment on the online version of the paper. Publisher's note: Springer Nature remains neutral with regard to jurisdictional claims in published maps and institutional affiliations. Correspondence and requests for materials should be addressed to A.H. (ase@gatech.edu).

Reviewer Information *Nature* thanks K. Lambrinou and R. Stieglitz for their contribution to the peer review of this work.

METHODS

Gas environment. To prevent oxidation of the liquid tin and to enable a wide selection of potential containment materials, the entire system was held in an inert N_2 environment. This resolved oxidation concerns from the beginning, rather than by constraining materials selection to oxidation-resistant materials or compatible coatings, and is fully compatible with large-scale industrial applications[30–32]. Here, extremely high temperatures are achieved inside the inert environment, but the boundary between the inert and natural oxygen-containing environment can remain cold because it is far outside the thermal insulation. This enabled the use of standard sealing approaches based on polymers (for example, silicone, backed by vacuum grease), which can be scalable and cost effective. Extended Data Fig. 2 shows examples of this sealing method. It was especially important for the oxygen content to be low, because the oxidation of Sn at a low O_2 pressure yields SnO, which melts completely at temperatures $\geq$1,313 K. Thus, any SnO that formed could become liquid in the circulation loop, but may partially freeze in colder sections, which can cause clogs.

The oxygen content was measured with a Zirox ZR5 zirconia-based sensor. By purging with ultrahigh-purity nitrogen and gettering with a small stirred pot of liquid tin, oxygen levels near 1×10^{-16} atm were consistently achieved, even reaching as low as 1×10^{-22} atm in some experiments. Extended Data Fig. 1 (see also Supplementary Data 2) shows the oxygen content versus time, with the change in slope due to the primary purging mechanism naturally switching from purging to gettering. At oxygen levels in this range, the remaining oxygen was able to react with the carbon and tin in the system with negligible oxide formation. However, quantifying the leak rate was also important. We determined it by leaving the chamber sealed over several days without a continuous purge and measuring the change in oxygen concentration. The leak rate was low (about 1×10^{-23} g O_2 s^{-1}) and would correspond to only about 1×10^{-13} g of SnO after 30 years. Even scaled to the length of seals in a representative industrial-scale plant (hundreds of metres of seal length), far less than 1 g of oxide would be formed over 30 years; the leak rate is reduced further by maintaining a slightly positive pressure in the chamber.

Material selection. Using the inert environment, materials such as graphite, tungsten and rhenium can be used at the target temperature, and remain stable as containment materials in contact with liquid tin (that is, they do not form thermodynamically stable compounds with liquid tin and exhibit negligible solubility in liquid tin at 1,373 K and 1 atm). (Although chromium also does not form stable solid compounds with tin at ambient pressure, its solubility in tin exceeds 12 at% above 1,373 K; ref. 50.) It is remarkable that even though graphite and tin are in the same column of the periodic table, they do not form stable chemical compounds at such temperatures and pressures[33,34]. Similarly, tungsten and rhenium are two exceptions on the periodic table, as the only high-melting-temperature (>3,373 K) metals that do not form stable compounds with tin and that exhibit negligible solubility in tin[51,52] (although rhenium is much more expensive than tungsten).

In this respect, tin is quite attractive in a general sense because it forms relatively weak oxides[53] and nitrides[54] and because it does not form a stable boride or carbide at ambient pressures. Consequently, it can be brought into contact with many oxides, nitrides, borides and carbides without appreciable reaction. Many ceramics are therefore compatible with liquid tin. Carbon (AR-14 Molded EDM graphite) was selected as the primary containment material because it is inexpensive, easily machinable and stable above 3,373 K. However, graphite has a relatively low fracture strength and is easily eroded, so it was not an optimal choice for wear surfaces. But using multiple materials at such high temperatures requires joints to be properly thermal-expansion matched so leaks do not develop and joints do not mechanically fail upon heating and cooling.

Pump system. Several pump options were considered, including centrifugal, axial, and external and internal gear pumps. Ultimately, an external gear pump was selected, which was tested to deliver at least 1 atm of pressure but is expected to be capable of 10 atm of head and up to 200 atm with high-precision fabrication[55]. This mechanical pump enabled separation of the pump and the electric motor that delivers the torque. Fundamentally, the idea was to separate high-temperature parts into one region and keep the electric motor in a cold region, with the two regions interconnected only by a series of mechanical members to transmit force. There are several options for tooth geometry in a gear pump[56]. Straight spur gear teeth were used because they enable relatively simple machining, which was especially important for this prototype and it is important in general for hard materials such as ceramics.

The Shapal pump was driven by a motor 30 cm away, outside the insulated region. The connection between the motor and pump used a flexible (helical) joint, custom jaw coupler, and external bearing to accommodate misalignment from thermal expansion. As shown in Fig. 2a–c, the motor shaft was extended with an insulating zirconia shaft. This bridged the $\geq$1,200 K temperature difference between the pump and motor and was supported by a tungsten sleeve bearing. The pump was mounted to a refractory brick base, which, in series with a cold plate, was mounted to a steel baseplate. Rigid mounting ensured that the pump body and motor did not rotate with respect to each other, so the only rotation was in the gears. Tungsten (hot isostatic pressed and machined) was used for high-temperature bolts because of its high tensile strength and toughness at the temperatures of interest. Here, another general design feature should be emphasized: because ceramics are generally much stronger in compression than in tension, we used the wider chemical compatibility of ceramics only where needed (for example, in contact with the fluid being pumped), with metal bolts and nuts used wherever tensile forces were applied. This enables metals not compatible with liquid tin, such as molybdenum, to be used, because there is no direct contact with the fluid being pumped.

To accommodate misalignment caused by thermal expansion—more than 1 mm of vertical growth occurred, as illustrated in Fig. 2d—the motor and pump were purposely offset from each other in the vertical direction at room temperature to account for the thermal expansion. This effect was achieved by first aligning the pump using standard shaft alignment styli and then shifting the pump vertically downwards with a precision linear stage. The pre-misalignment targeted an average operation temperature of 1,273 K, based on simulated thermal growth of 1.02 mm. By purposefully misaligning the pump at room temperature, the pump comes into alignment when heated, minimizing the stress on the ceramic components. This approach is complemented by the angularly flexible, yet radially constrained, shaft set-up involving the tungsten sleeve bearing. A detailed description of this system is available elsewhere[57].

Sealing. Pump seals are usually polymer-based, owing to their high compliance against sealing surfaces, but they cannot survive the extreme temperatures considered here. Mechanical face seals are a potential solution, although they require the added complexity of multiple components and extreme precision. Nonetheless, this is potentially an approach to be pursued in future work, because the sealing materials used can have wider chemical compatibility than graphite. This approach also typically depends on a constant leak rate to lubricate the seal, which could lead to containment and freezing issues but could conceivably be managed. Here we instead leverage the compliance of graphite. The seal along the gear shaft that prevents the liquid tin from escaping the high-pressure region inside the pump to the lower-pressure outside gas environment is made of graphite packing material (Palmetto 5000). Sealing is achieved through radial expansion when the seal is compressed axially (see Fig. 3a). Although the seal is designed to slowly wear away over time, it can be continually and even automatically tightened, by using Belleville washers or more elaborate, actively actuated designs.

Static seals in this system were achieved in two ways: graphite reaction bonding and graphite ferrule/foil compression. For example, the pump gear cavity was enclosed in a two-part body (Fig. 2a) and the space between the two parts was sealed using a graphoil (graphite) sheet body seal compressed by tungsten bolts. Removable fluid connections relied on the compression of graphite ferrules (Fig. 3b), which provided a reliable seal. For permanent connections, reaction bonding was used, which can deliver a compact, reliable connection for many refractory materials (such as C, Al_2O_3, AlN, SiC and ZrO_2) using commercial products from, for example, Cotronics, Aremco, or others. For example, the pump fittings shown on the left of Fig. 3b are bonded in this way, using Ceramabond 865. Similarly, the reservoir outlet pipe (Fig. 1) is bonded with Resbond 931. These bonding processes require low curing temperatures (about 400 K) compared to the temperature limit of the final material (>1,673 K) and can easily be applied in the field. The process by which the ceramic pipes were sealed (as described in Fig. 3 or via reaction bonding) is less complex than welding, suggesting that the labour costs associated with assembling and installing such systems may be similar to that of standard metal-based approaches. This is particularly important for the economics of new ideas enabled by our technology.

Thermal management. The system was insulated with ZIRCAR Ceramics AB alumina blanket (95% alumina) and rigid ZAL-15AA (97% alumina) insulation. MICROSIL microporous silica blanket and rigid insulation was used external to the alumina for its very low thermal conductivity (0.03 W m^{-1} K^{-1}) because its use is limited to 1,273 K, above which it would sinter and lose its insulating properties. Heat was applied primarily via a 10-kW-maximum high-frequency (100–500 kHz) induction furnace, with a water-cooled copper loop brought within 3 cm of the 1,473 K reservoir, separated only by rigid insulation. In addition to the induction furnace, heating to other portions of the circulation loop was provided by Kanthal resistive heaters. The inductive heating enables extremely high temperatures because it generates heat within the high-temperature graphite reservoir directly. The extremely high convective heat transfer coefficient of the liquid metal effectively distributed the heat throughout the system, which allowed for a simple, reliable and precisely controllable set-up.

Flow-rate measurement. To quantify flow rate, we designed a weight-based flow meter. The equilibrium mass in this flow meter, which consisted of a reservoir with

a base orifice, was a function of the flow rate at the inlet. By measuring the weight of this reservoir over time, when allowed to drain without inflow, a calibration curve for the *in situ* flow rate was developed. This test involved first running the pump at a high flow rate to fill the flow meter (see Extended Data Fig. 4). Then, once filled, the pump was immediately stopped and the liquid, the weight of which was being tracked, was allowed to drain. As the liquid drained, the mass of the flow meter decreased, and by numerically differentiating the measured mass with respect to time, the mass flow rate exiting the topmost reservoir was determined. Because both the mass and mass flow rate were known at each instant, by eliminating the time variable, the mass flow rate versus mass was determined (see Extended Data Fig. 3 and Supplemental Data 3). The basic principle is that the transient rate at which tin drains through the orifice at a given measured weight is equivalent to the steady-state flow rate that would maintain that same height and weight when there is a steady-state inflow and outflow (that is, a steady height and weight measurement occurs when the rate at which fluid flows in is equal to the rate at which it flows out). Subsequent testing showed that the performance of this flow meter matched well with predictions based on the application of Bernoulli's equation, namely, that the flow rate was proportional to the square-root of fluid mass (Extended Data Fig. 3a).

The large size of the entire flow meter system (see Extended Data Fig. 4) made it difficult to simultaneously meter the flow and reach the target temperature of 1,473 K, owing to increased heat losses. In light of this problem, an alternative visual flow meter was used for higher-temperature experiments (1,473 K), and even higher temperatures (>1,673 K) were obtained by not using a flow meter at all. The visual flow meter is shown in each of its three flow regimes in Extended Data Fig. 3b–d. In essence, the visual flow meter shows liquid metal exiting through different numbers of orifices, depending on the rate of inflow. The target for these experiments was to have flow out of two of the three orifices, as illustrated in Extended Data Fig. 3, which corresponded to a flow rate of 24–108 g s^{-1}.

To calibrate the visual flow meter, the mass flow meter was positioned above it. This arrangement (Extended Data Fig. 4) allowed the reading from the mass flow meter to be related to the number of streams of liquid observed in the visual flow meter directly. Using this approach, the weight-based flow meter was used to determine the flow-rate thresholds between the observation of two (24 g s^{-1}) and three (108 g s^{-1}) streams from the visual flow meter. Here, we define an outlet to be activated when the tin stream was continuous (not droplets). To account for the error in this visual measurement, the lower bound (24 g s^{-1}) is the minimum observed mass flow rate that resulted in continuous flow, rather than the average.

Mechanical issues and wear. During initial testing, many challenges were encountered. Before the successful test, we encountered issues with the insulating shaft bearing, shaft alignment and wear. Because of the system temperature, only a limited set of materials could be used for the bearing and an even more limited set of commercially available bearings exists. After evaluating many options, including commercially available ceramic ball bearings, we chose a tungsten sleeve bearing specifically designed to constrain the shaft only radially, and not angularly. This thin tungsten bearing is shown in Fig. 2a and has a full fillet on the inner surface of the bearing so that, at small angles, the shaft is free to angularly deflect (see Extended Data Fig. 5). This constraint is key because as the pump grows vertically the ZrO_2 shaft deflects angularly; a typical sleeve or ball bearing would constrain this angle, resulting in high stress on the bearing.

Another main challenge is the excessive wear rates experienced at Shapal–Shapal interfaces. Besides the low hardness of Shapal, a major source of wear is third-particle abrasion caused by abraded AlN particles grinding the much softer BN, which exposes more AlN to be abraded[58]. This issue is specific to this composite material. Although this issue can be resolved by using a harder, homogeneous, fine-grain ceramic such as alumina, several other factors should be considered for proper tribological design.

Because sleeve bearings are used for the pump gears, they experience sliding wear. This wear rate is exacerbated if the bearing is not properly lubricated. During initial tests, the wear rate of the bearing–shaft interface (see Extended Data Fig. 5a) was found to be very severe (a wear coefficient of about 3×10^{-1}), but after polishing these surfaces the wear rate was reduced by a factor of 30, to 1×10^{-2}. The target of these highly polished surfaces is to enable full hydrodynamic film lubrication, where there is no contact between the bearing and the shaft. Although asperity contact was clearly reduced, this target was probably not achieved because of the small size and limited precision of the pump components. Another factor that can prevent full-film lubrication is the linear speed of the shaft surface, which in this experiment was low (about 0.1 m s^{-1}). Here, the shaft speed was maintained at a low speed to prevent splashing of the liquid metal at the various free surfaces in the flow meters and the reservoir. Splashing was avoided for safety reasons, but does not limit such devices in a real application. In an industrial-scale application, electromagnetic flow meters can be used and view ports with free surfaces are probably not necessary, thus eliminating the associated safety concern.

In addition to bearing wear, the gear teeth also experienced substantial wear, as shown in Fig. 5 and quantified in Extended Data Table 1. The causes here are similar to those for bearing wear; however, to achieve low wear rate, elastohydrodynamic lubrication is ideal[40,59]. If this regime is met, which requires precise, polished gears and sufficient shaft speed, then the gear teeth do not contact directly. Instead, they remain separated by a very thin layer of liquid, which requires a finite time to deform when driven by a finite force. Such operation would be ideal and would prolong the operational life tremendously.

To achieve these ideal wear regimes, an alternate pump material should be used, and potentially another geometry as well. For example, Al_2O_3, ZrO_2, Si_3N_4 and SiC are compatible materials that can have wear rates 2–5 orders of magnitude lower than what Shapal experienced (wear coefficients as low as 1×10^{-7} compared to about 1×10^{-2}), even when marginally lubricated[60,61]. If full film lubrication is achieved, then the wear rate can be reduced by an additional 2–3 orders of magnitude (wear coefficients as low as 1×10^{-10}), enabling continuous operation for many years[40]. Similarly, a centrifugal pump or a gear pump with herringbone gears can reduce the wear rate. To enable the pumping of a broad range of liquid metals, the graphite used in the system could be replaced with a less reactive material. The most challenging component to replace is the shaft seal, although several woven ceramic fibres could possibly be used instead of graphite. To enable the most challenging applications, such as pumping up a concentrated solar power tower, multiple pumps could be used in series and the pump type could be changed.

Data availability. All data generated or analysed during this study are available from the corresponding author on reasonable request. Data reported are available in the paper and its Supplementary Information.

50. Venkatraman, M. & Neumann, J. P. The Cr−Sn (chromium–tin) system. *J. Phase Equilibria* **9,** 159–162 (1988).
51. Predel, B. *Sn–W (Tin–Tungsten)* http://doi.org/10.1007/10551312_2771 (Springer, 1998).
52. Massalski, T. B., Okamoto, H., Subramanian, P. R. & Kacprzak, L. (eds) *Binary Alloy Phase Diagrams* 2nd edn, 723–806 (ASM International, 1990).
53. House, J. E. & House, K. A. *Descriptive Inorganic Chemistry* 3rd edn, 177–196 (Academic Press, 2016).
54. Lima, R. S., Dionísio, P. H., Moro, J. T., Schreiner, W. H. & Achete, C. Thermal evolution and stability of a tin nitride obtained by reactive sputtering. *Hyperfine Interact.* **83,** 315–319 (1994).
55. Casoli, P., Vacca, A. & Berta, G. L. Optimization of relevant design parameters of external gear pumps. *Proc. JFPS Int. Symp. Fluid Power* **2008,** 277–282 (2008).
56. Amani, A., Spitas, C. & Spitas, V. Generalised non-dimensional multi-parametric involute spur gear design model considering manufacturability and geometrical compatibility. *Mechanism Mach. Theory* **109,** 250–277 (2017).
57. Amy, C. *Liquid Metal Pumps for Enabling Heat Transfer at Extreme Temperatures* MSc thesis, Georgia Institute of Technology (2017).
58. He, X., Gong, Q., Guo, Y. & Liu, J. Microstructure and properties of AlN-BN composites prepared by sparking plasma sintering method. *J. Alloys Compd.* **675,** 168–173 (2016).
59. Mucchi, E., Agazzi, A., D'Elia, G. & Dalpiaz, G. On the wear and lubrication regime in variable displacement vane pumps. *Wear* **306,** 36–46 (2013).
60. Peterson, M. B. & Winer, W. O. (eds) *Wear Control Handbook* 35–80 (American Society of Mechanical Engineers, 1980).
61. Kato, K. Tribology of ceramics. *Wear* **136,** 117–133 (1990).

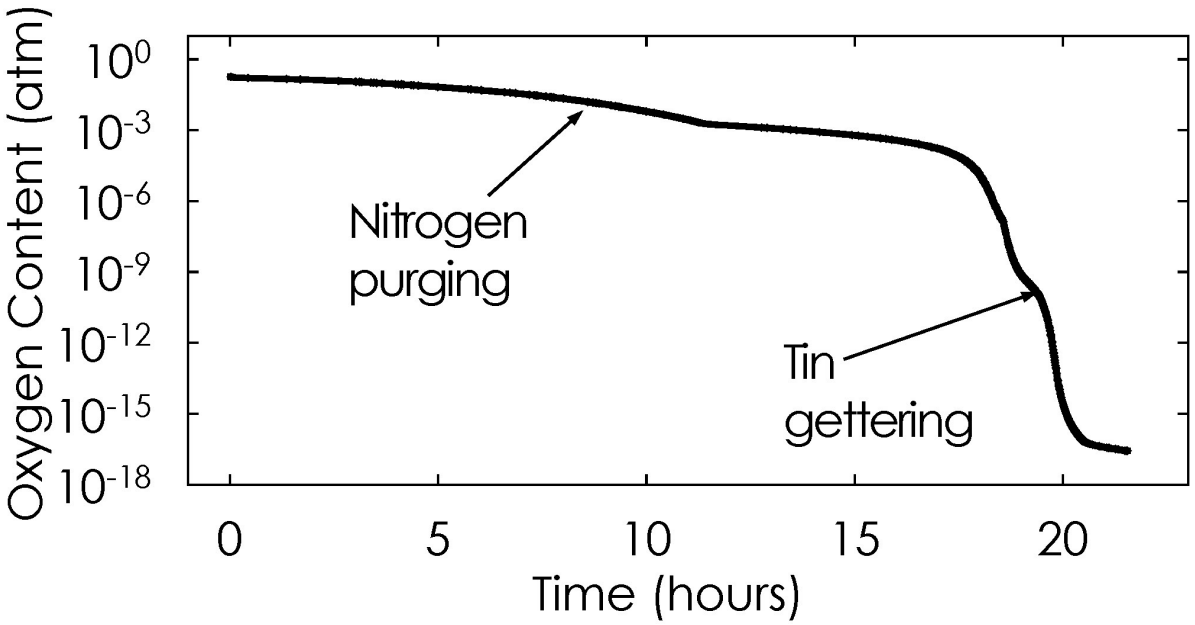

Extended Data Figure 1 | Oxygen content over time in preparation for the experiment. After 17 h of nitrogen purging, the oxygen level decreased sufficiently for tin gettering to take over as the dominant oxygen reduction mechanism.

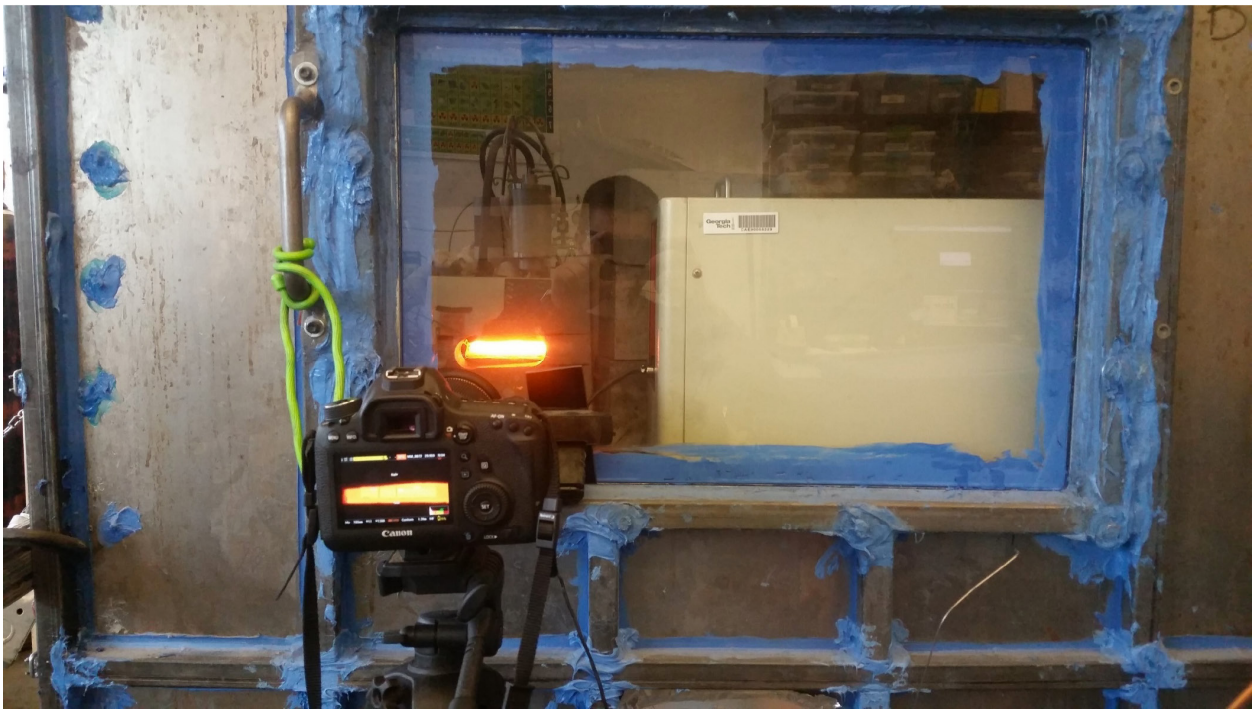

Extended Data Figure 2 | Chamber view including seals and the visual flow meter port. Seals were achieved by first applying room-temperature vulcanization (RTV) silicone (blue) and then applying vacuum grease. The viewport is the glowing orange slotted hole shown in the insulation. The camera position is shown as a reference to the image in Fig. 4.

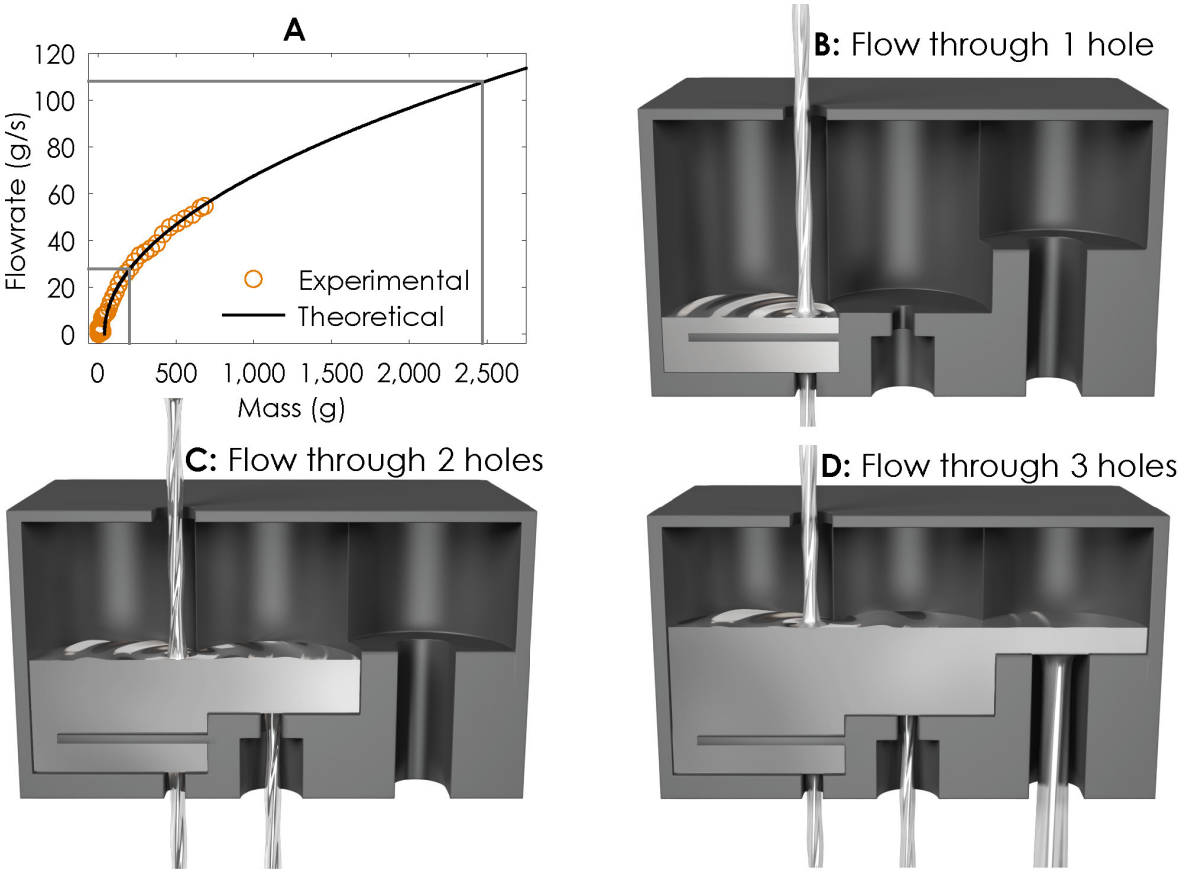

Extended Data Figure 3 | Design and calibration of the visual flow meter. a, Measured flow rate versus mass in the flow meter (mass uncertainty is ±5 g). The grey boxes identify the flow regimes, with the smaller box corresponding to transition from one- to two-hole flow, and the larger box corresponding to transition from two- to three-hole flow. The theoretical curve is determined using Bernoulli's equation, whereby the flow rate is proportional to the square-root of mass. **b**–**d**, Illustrations of the three possible flow regimes that can be detected by the visual flow meter.

Extended Data Figure 4 | Experimental set-up of the calibration of the visual flow meter. The weight-based flow meter was positioned above the visual flow meter and the pump speed was adjusted until the desired flow (for example, through only two outlets or through three outlets) was achieved. Under these conditions, flow was monitored from both flow meters so that the quantitative information from the weight-based flow meter could be related to the qualitative information from the visual flow meter.

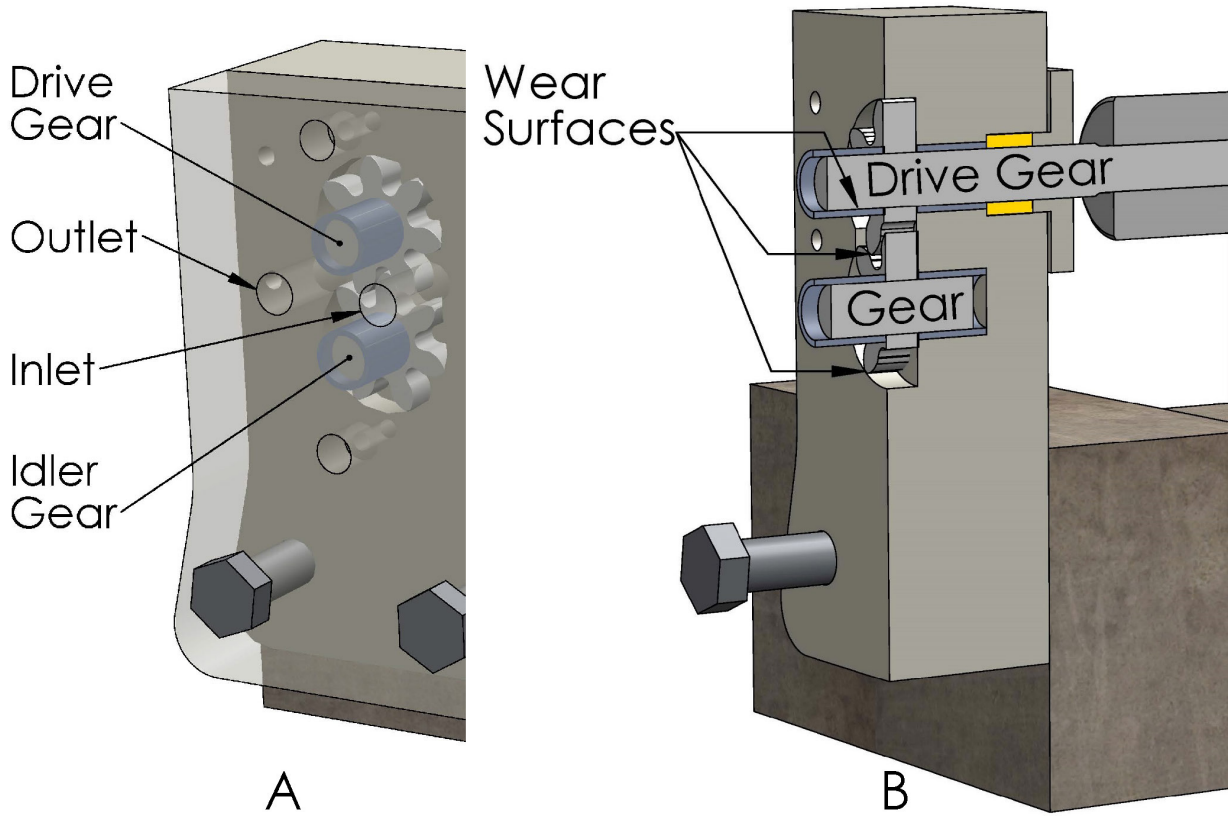

Extended Data Figure 5 | Internal features of the gear pump, including wear surfaces. a, View of the internal geometry of the pump system. **b**, View of the wear surfaces of the pump gear. Although wear occurred on most dynamic surfaces, the most extensive wear occurred on the gear shafts. Wear allows the gear tips to contact the pump body, which results in performance-reducing wear on the tips of the gear teeth.

Extended Data Table 1 | Amount and coefficients of wear for the pump gears after 72 h

Dimension	Baseline	Drive	Drive loss	Idler	Idler loss	Unit
Tooth width	6.78	5.82	0.97	6.68	0.10	mm
Gear Thickness	8.89	8.66	0.23	8.84	0.05	mm
Gear Diameter (3 pt)	36.42	36.20	0.23	36.07	0.36	mm
Shaft Diameter	12.70	12.59	0.11	12.54	0.16	mm
Gear Wear Coefficient			2.85E-02		5.41E-03	unitless
Shaft Wear Coefficient			3.68E-02		4.41E-02	unitless

72 h corresponds to about 1,000,000 revolutions. The wear coefficient is calculated using the Archard equation: $K = QH/W$, where Q is the wear rate in volume per distance slid, H is the material hardness and W is the applied force (estimated on the basis of pressure head delivered and an estimated pump efficiency of 50%). Although most wear occurred at the gear teeth, the wear that occurred at the radial gear tip was most detrimental to performance because it allowed fluid to leak around the teeth. The outer surface of the radial gear tip contacts the pump body only as the shaft wears; minimizing the wear rates of the shaft and bearing is therefore key.